Geochemical volcano monitoring

Alessandro Aiuppa[1], Mariano Agusto[2], Patrick Allard[3], Simon Carn[4], Maarten J. de Moor[5], Salvatore Inguaggiato[6], Agnes Mazot[7], Y. Moussallam[8], and Patricia Nadeau[9]

[1]Dipartimento di Scienze della Terra e del Mare, Università di Palermo, Palermo, Italy
[2]Universidad de Buenos Aires (UBA), National Scientific and Technical Research Council (CONICET), Buenos Aires, Argentina
[3]Institute de Physique du Globe (IPGP), Paris, France
[4]Geological and Mining Engineering and Sciences, Michigan Technological University, USA
[5]OVSICORI, Universidad Nacional, Costa Rica
[6]Istituto Nazionale di Geofisica e Vulcanologia, Sezione di Palermo, Palermo, Italy
[7]GNS Science, New Zeeland
[8]Lamont-Doherty Earth Observatory, Columbia University, New York, USA
[9]USGS Hawaiian Volcano Observatory, Hilo, USA

Abstract - *The geochemistry of volcanic fluids is increasingly employed at volcano observatories worldwide to assess volcano activity state, and eruption potential. Here, we review the state-of-the-art in the field, with a primary focus on the most recent developments in instrumental gas monitoring that have rendered geochemistry an increasingly effective eruption-forecasting tool. We describe the main geochemical techniques, from both ground and space, and how they each contribute to volcano monitoring. By presenting some selected case studies, we demonstrate that geochemical monitoring strategies need to adapt as volcanic activity state evolves during unrest and in the run-up to eruption. Modern gas-monitoring networks need to integrate different instrumental tools and require collection of a variety of gas-related signals if any subtle change in volcano behavior is to be captured in a timely manner.*

Keywords: *fluid geochemistry; geochemical monitoring; volcanic gases; magmatic degassing; magmatic gas-hydrothermal interactions; direct sampling; remote sensing; volcanic plumes; soil degassing; crater lakes.*

1. Introduction.

Volcanoes emit magma-sourced volatiles through a variety of fluid manifestations, ranging from (i) large atmospheric plumes released by open-vent volcanoes to (ii) fumaroles, steaming grounds/mud pools, hot/cold spring waters, and degassing soils that represent the dominant emission forms at closed-vent, dormant volcanoes [1]. Geochemical monitoring is useful because volcanic fluids exhibit temporal changes in chemistry and mass flux that reflect critical changes in the magma and its surroundings, providing insights into the volcano and its potential for eruption.

The chemistry of volcanic fluids has now been investigated for more than a century, initially instigated by the curiosity of key volcano chemist pioneers [2]. However, it was not until the 1970s that geochemical observations became systematic enough to emerge as a potential tool for volcanic eruption forecasting [3]. It is today universally accepted that, in addition to contributing to volcano monitoring, fluid geochemistry is central to understanding magma degassing processes [4], the architecture of magma feeding systems [4, **add QR to Further Readings**], and estimation of the T-P-X conditions of volcano-hosted hydrothermal systems and their interactions with magmatic fluids [5]. Modern fluid geochemistry also contributes to sustainable development by offering a relatively inexpensive volcano monitoring tool, even in countries where volcanology is a still emerging field. Installation/maintenance of geochemical instrumentation remains an issue, however, especially for volcano observatories monitoring remote, poorly accessible volcanoes.

Broadly speaking, geochemical monitoring requires time series to be acquired for the composition and/or the flux (ideally both) of volcanic fluids. With a robust dataset in hands, and in combination with evidence streaming from other disciplines, geochemists interpret observed geochemical changes in reference to a conceptual model of volcano behavior (Fig. 1), from which they attempt to resolve any sign of volcano unrest or potential eruption.

Geochemical observations can be obtained via either (i) periodic surveys involving direct sampling or in-situ field measurement of fluids [3] or (ii) near-continuous records from fully automated field-deployed instruments [6-8]. Although the two strategies are very complementary, the second is intrinsically more beneficial for capturing the rapidly evolving dynamics of soon-to-erupt volcanoes. Periodic surveys are more appropriate for volcanoes with longer repose times, for remote volcanoes where instrument installation and maintenance can be challenging, and for measuring the whole chemical-isotopic spectrum of volcanic fluids. Over the years, geochemical monitoring has progressively transitioned toward the implementation of permanent instrumental networks, and this evolution is well represented in the two previous editions of the Encyclopedia of Volcanoes. In the first edition (2000), Delmelle and Stix [9] discussed the processes governing the temporal variability of volcanic gas composition mostly relying on the results of periodic direct sampling of fumaroles. In the same volume, Stix and Gaonach [10] elaborated on initial instrumental attempts to remotely measure plume composition

86 (by Fourier Transform Infrared Spectroscopy, FTIR), and the volcanic SO_2 flux
87 from either ground (using the Correlation Spectrometer, COSPEC) and space
88 (using the Total Ozone Mapping Spectrometer, TOMS). In the second edition,
89 Fischer and Chiodini [5] still heavily elaborated upon the results of direct fumarole
90 sampling, discussing isotopic evidence for the origin of elements (C-H-O-S-N-
91 halogens-noble gases) in volcanic gases, and presenting a comprehensive
92 discussion on thermodynamic techniques used to estimate hydrothermal P-T
93 conditions from hydrothermal gas equilibria in the H_2O-H_2-CO_2-CO-CH_4 system
94 (the reader is referred to this study for a detailed discussion of both topics).
95 However, they also increasingly discussed the application of instrumental
96 techniques in geochemical volcano monitoring.

97 The core focus of the present chapter is to review the most recent technological
98 and science advances in volcanic gas monitoring.

99 2. **Drivers of change: what controls geochemical changes.**

100 Interpreting the time series streamed by a geochemical volcano monitoring
101 network requires that a coherent understanding is available for the processes that
102 drive change in fluid chemistry/flux (Fig. 1). This knowledge also serves as a guide
103 for the establishment of the monitoring network, and for selecting the ideal
104 parameters to monitor. Key to success is a robust knowledge of baseline
105 composition/flux levels (to be acquired during volcano repose or background
106 eruptive activity) – this is needed to identify change. We review below the key
107 drivers of change at play at volcanoes.

108 2.1 Strong Volcanic Gas Emitters: change due to magmatic degassing processes.

109 With the term Strong Volcanic Gas Emitters (SVGE), we refer to those volcanoes
110 whose gas emissions have regularly (or frequently) been detected from space in
111 the last decades of satellite observations. This category includes a broad spectrum
112 of volcanoes, such as (i) open-vent, persistently degassing mafic volcanoes and
113 (ii) more silicic volcanoes that are (or have recently been) in eruption or are soon
114 to erupt, and therefore host high-temperature (>> 600 °C) crater fumarole fields
115 (Fig. 1a). At these volcanoes, the critical process that imparts compositional
116 variability in volcanic fluids is the selective/sequential vapor partitioning of the
117 various volatiles during magma degassing (Fig. 1a). Magma degassing, the
118 process through which volatiles exsolve from silicate melt and separate into a
119 vapor phase (bubbles), is a universal process associated with magma ascent and
120 decompression (decompressional degassing) and/or crystallization (second
121 boiling) [4,6]. At any P-T-X condition, the magmatic volatile species have distinct
122 solubilities and vapor/melt partitioning behaviors. The less soluble volatiles (Ar,
123 N_2>CO_2 >He) partition into the volatile phase earlier (deeper) than more soluble
124 ones ($H_2O \approx S <$ halogens) [6], so the chemical ratios between the species evolve
125 during magma decompression (ascent) [11]. Geochemists exploit this degassing
126 pattern to monitor changes in magma degassing depth/conditions from changes in
127 gas ratios (e.g., Ar/CO_2, CO_2/He, CO_2/S, CO_2/H_2O, S/Cl) in monitored surface
128 fluids. This directly applies when surface fluids are purely magmatic in nature, i.e.,

129 directly derived from magma without any re-equilibration or hydrothermal alteration
130 (see below). Solubility-dependent degassing patterns are thus mainly explored in
131 magmatic emissions from SVGE (Fig. 1a), or in WVGE that are transitioning into
132 eruption (where degassing signals may be more confused as masked by
133 hydrothermal interactions, see below). Magmatic gases are essentially mixtures of
134 major species H_2O, CO_2, and SO_2 (H_2S normally makes a small fraction of total
135 sulfur S_t: Fig. 1b), plus a plethora of minor and trace species. While inter-volcano
136 variations in H_2O-CO_2-SO_2 proportions mostly reflect different geodynamic setting
137 (that is, melt compositions and volatile contents; [4]), temporal changes at
138 individual volcanoes have been shown to be caused by and indicative of changing
139 magma degassing conditions. In particular, increasing CO_2/SO_2 ratios have now
140 been observed prior to eruption at many mafic and silicic volcanoes worldwide.
141 This reflects the precursory surface release of deeply exsolved CO_2-rich gas,
142 separately ascending from soon-to-erupt mafic magma at depth [8, 11] (Fig. 1a,
143 b).

144 In addition to chemical composition, gas fluxes (e.g., the mass of gas emitted per
145 unit time) also change in response to pre-eruptive magma accumulation/ascent
146 and degassing. This is easily understood in the specific case of the SO_2 flux (ΦSO_2,
147 in kg/s), the most easily measurable volatile (see 3.3), from the relationship:

148 $$\emptyset_{SO2} = \ Q_{in} \cdot 2\Delta X_S \cdot (1-x) \cdot \rho_m$$

149 where Q_{in} is the magma input rate (in m^3/s) above the level (depth/pressure) at
150 which effective sulfur degassing starts (typically 4-9 km below the volcano top for
151 mafic magma [6]), ΔX_S is the bulk mass loss of elemental sulfur upon degassing
152 (e.g., the difference between parental melt and residual S content in degassed
153 magma), and x and ρ_m are melt crystallinity and density (in kg/m^3) (the coefficient
154 2 = 64/32 is required to covert S mass into SO_2 mass). When magma supply (Q_{in})
155 to the volcano feeding system increases in the eruption run-up, the SO_2 flux
156 escalates in advance to magma eruption, either because gas bubbles are buoyant
157 enough to separately ascend through the melt or because they can escape via a
158 permeable gas bubble network. Note that the same equation is used to convert
159 measured SO_2 fluxes into Q_{in} using petrological estimates of S contents in melt
160 inclusions and matrix glasses [4].

161 2.2 Weak Volcanic Gas Emitters: change due to magmatic-hydrothermal
162 reactions.

163 Closed-vent, dormant/quiescent stratovolcanoes and calderas (Fig. 1c) are
164 normally classified as Weak Volcanic Gas Emitters (WVGE) as they typically lack
165 large atmospheric plumes that can be detected from space. Their most visible
166 degassing manifestations are relatively cold (typically close-to-boiling
167 temperature) fumaroles and steaming grounds/soils [1]. During volcano repose,
168 these manifestations typically exhibit stable hydrothermal signatures, being
169 dominated by steam (generally > 90 mol. %) plus 1-10 mol% gas essentially
170 consisting of a CO_2+H_2S mixture [5, 9], plus minor N_2, Ar, H_2, CH_4, and CO, but no
171 (or minimal) SO_2 and HCl (exceptions of SO_2 and HCl-rich hydrothermal gases

172 exist, however). These S-poor (Fig. 1b) hydrothermal vapors are generally formed
173 by boiling of (meteoric water- or seawater-fed) aquifers heated by a magma source
174 at depth, but they usually contain a magmatic volatile component as well, as
175 evidenced by isotopic evidence (primarily $^{13}C/^{12}C$ and $^{3}He/^{4}He$ ratios; [6]). Hence,
176 at WVGE volcanoes, chemical changes are mainly driven by the extent and
177 dynamics of hydrothermal-magmatic fluid interactions [11]. If the volcano becomes
178 restless, geochemists carefully examine fumarole compositional time series to
179 identify any increase in the magmatic gas proportion, as indicated for example by
180 increasingly CO_2-S-rich and less water-rich compositions (Fig. 1b). Complications
181 arise, however, as the magmatic S supply can be masked by scrubbing (the
182 sequestration of SO_2 and H_2S - and other reactive gas species - into hydrothermal
183 solutions/minerals, owing to their high water solubility and reactivity to host rocks),
184 and because sulfur may instead be contributed by destabilization of S-bearing
185 hydrothermal minerals in the volcano heating phase (Fig. 1c). This makes inert
186 gases (N_2, noble gases) and their isotopic ratios more sensitive tracers of an
187 increasingly magmatic signature of fluids [5]. Compositional change is also
188 determined by evolving hydrothermal P-T conditions, driven by increasing supply
189 of hot magmatic gases. This evolution can be monitored by modeling H_2O-H_2-CO_2-
190 CO-CH_4 equilibria (Fig. 1d) that are extremely sensitive to P-T-redox conditions
191 [5]. While remote SO_2 flux measurements are ineffective during quiescence and
192 early unrest phases at WVGE, due to nil or weak SO_2 release, soil gas monitoring
193 and airborne plume CO_2 surveys can allow early detection of increasing supply of
194 magma-sourced CO_2.

195 ## 3. Sentinels of change: techniques in geochemical monitoring

196 An appropriate volcano monitoring strategy requires the combination of different
197 techniques into an integrated observational network (Fig. 2). It is important to keep
198 in mind that the fluid manifestations vary with volcanic activity status and style [1],
199 implying that the choice of methods/instrumentations to prioritize may vary as a
200 volcano becomes increasingly restless (Fig. 2). This section describes the principal
201 geochemical techniques used and their respective contributions to volcano
202 monitoring (with some selected case studies).

203 3.1. Fumarole direct sampling.

204 Although gas monitoring is increasingly realized using real-time instrumental
205 networks (Fig. 2), direct sampling remains an invaluable source of information, as
206 it is the only tool that allows for a full characterization of the volcanic gas
207 composition, including minor and trace elements and isotopes. Direct sampling
208 involves collection of fumarole gases using Giggenbach's alkaline solution method
209 [3, 5]. In this process, fumarolic gas stream is channeled (via a quartz tube) into a
210 pre-evacuated and pre-weighed flask filled with 4 M NaOH. Fumarolic gases
211 bubble through the alkaline solution, causing water vapor to condense, and CO_2
212 and acidic gases (HCl, HF and S species) to dissolve in the solution. Non-
213 condensable gases (H_2, N_2, CO, and CH_4) and noble gases are hence
214 concentrated in the flask headspace.

215 Water, the most abundant magmatic volatiles, is difficult to measure in plumes (cf.
216 3.2), because of the high and variable atmospheric background. Hence, direct
217 sampling is the key tool to reliably detect the gas/steam (CO_2/H_2O) ratio increase
218 [12] that typically tracks the increasing magmatic (over hydrothermal) fluid
219 contribution as a volcano becomes restless (see also the Turrialba example [13]
220 illustrated in Figure 1b). Direct sampling can also capture hydrogen and oxygen
221 isotope compositions normally becoming increasingly heavy (δD and $\delta^{18}O$
222 becoming more positive) as fumarolic steam transitions to having a greater
223 proportion of magmatic relative to meteoric water [14]. Resolving the magmatic vs.
224 non-magmatic fluid (meteoric, atmospheric, biogenic) contributions becomes
225 especially effective when a multi-isotope approach is employed, in which tracers
226 such as C ($\delta^{13}C$; Fig. 3), N ($\delta^{15}N$), He ($^3He/^4He$), and Ar ($^{40}Ar/^{36}Ar$) isotopes (to cite
227 only the most frequently used) are measured in concert [6]. The isotopic
228 compositions of such elements allow quantification of the magmatic gas influx, to
229 infer volatile origin, and to characterize the physico-chemical processes of magma
230 degassing, gas migration, and interaction with groundwaters. Noble gases
231 ($^3He/^4He$, $^4He/^{20}Ne$, and $^{40}Ar/^{36}Ar$ ratios) are especially useful in this exercise,
232 because of their inert nature, and because of the contrasting signatures of
233 magmatic, crustal and atmospheric sources.

234 In addition to isotopes, a series of chemical tracers are effectively monitored by
235 direct sampling to track unrest, and potentially forecast activity resumption at
236 closed-vent volcanoes. For example, as magma migrates toward the surface,
237 scrubbing of magmatic S and Cl by hydrothermal reactions [15] will be reduced or
238 minimized, which can be detected by decreasing CO_2/S ratios (Fig. 1, 4), change
239 in S speciation (increases of magmatic SO_2 over hydrothermal H_2S) and increasing
240 halogens ($HCl+HF/CO_2$) (Figs. 3 and 4). Also, the minor carbon species, and the
241 proportion relative to CO_2 are especially useful as they are sensitive to temporal
242 changes in pressure and temperature conditions of the hydrothermal system. As
243 a rule of thumb, the CO/CO_2 and CO_2/CH_4 ratios both increase (Fig. 1d) as the
244 magmatic gas influx increases, and hence the hydrothermal system is driven to
245 higher temperature and eventually more oxidized (magmatic) conditions.

246 *Case study box: Peteroa and Pico de Fogo*

247 Over the past decade, extensive crater fumarole time series have been obtained
248 by direct sampling that have not only identified precursors to eruption, but also
249 revealed the intricate processes that control volcano dynamics. Direct sampling
250 has made significant strides in understanding the compositional variations before
251 and during eruptions. Two notable cases in which gas parameters have
252 contributed to effectively identify processes and likelihood of eruption are those of
253 Peteroa volcano (Argentina-Chile) and Pico do Fogo (Cape Verde) (Figure 3).

254 Peteroa is a typical andesitic WVGE stratovolcano with fumaroles at near boiling
255 temperatures. During 2010 to present, the volcano has experienced two mildly
256 explosive (Volcanic Explosivity Index, VEI =2) eruptions in 2011 and 2018-2019
257 (Fig. 3a). Regular fumarole direct sampling contributed to tracking the quiescence-
258 to-eruption transition by distinguishing clear switches from hydrothermal to

259 magmatic compositions. During quiescence, gas composition was typically in the
260 hydrothermal domain, as indicated by low HCl/CO_2 and SO_2/H_2S ratios (Fig. 3a).
261 In contrast, in the pre-, syn-, and post-eruptive phases, SO_2, HCl, and HF
262 increased significantly, causing the SO_2/H_2S, HF/CO_2, and HCl/CO_2 to
263 simultaneously increase by orders of magnitudes (Fig. 3a), and implying minimal
264 (or reduced) magmatic gas scrubbing and more oxidizing redox conditions (as
265 typical of magmatic conditions). This redox evolution before the phreatomagmatic
266 eruption was also detected using the CH_4/Ar ratio. During quiescence, the CH_4/Ar
267 ratio was high, indicating reducing conditions and low temperatures (Ar was largely
268 meteoric Ar, as indicated by $^{40}Ar/^{36}Ar$ ratios slightly above the 295 air ratio). The
269 CH_4/Ar ratio then decreased in the 2018-2019 magmatic phase (Fig. 3a), indicating
270 CH_4 was depleted at a faster rate (prevalence of oxidizing, magmatic conditions)
271 relative to Ar.

272 Similar changes in gas composition were observed before the 2014-2015 eruption
273 of Pico do Fogo volcano [17] (Figure 3b), a mafic alkaline volcano in the Cape
274 Verde archipelago hosting a summit hydrothermal system feeding a swarm of
275 crater fumaroles with temperatures up to 350°C. The fumarolic CO/CO_2 and
276 H_2/CO_2 ratios started to increase in 2009-2010 (marking the onset of a "magmatic
277 reactivation" phase). These variations were interpreted [17] as caused by an
278 escalating input of deeply sourced, CO_2-rich magmatic gases that ultimately
279 caused heating of the hydrothermal system. This heating phase manifested in a
280 remarkable increase of estimated equilibrium temperatures (Eq.T in Figure 3b),
281 from circa 200 to circa 500°C (as inferred from CH_4-CO-CO_2 geothermal gas
282 geothermometer [5]). The isotopic composition of $δ^{13}C–CO_2$ (in ‰ vs. VPDB, Fig.
283 3b) peaked at the eruption onset, implying involvement of an isotopically heavier
284 (more magmatic) CO_2 source, associated with the volatile-rich erupting magma.

285 3.2. In-situ plume measurements

286 At open-vent volcanoes, direct fumarole sampling becomes increasingly
287 ineffective since the gas output is dominantly sustained by large atmospheric
288 plumes [1]. Monitoring hence requires plume measurements. In-situ
289 measurements are made after the gas has exited the crater and been diluted by
290 atmosphere. The two most common in-situ plume techniques are chemical traps
291 and Multi-GAS measurements. Both techniques rely on a pump to draw volcanic
292 gases into the instrument.

293 Chemical traps use compounds that react with acid volcanic gas species to take
294 samples of volcanic plumes. The most used technique is the filter pack method,
295 whereby plume gas is pumped through a series of filters impregnated with alkaline
296 solutions such as K_2CO_3 or NaOH with glycerol to enhance the absorption
297 efficiency. This method is convenient for rapid sampling of plumes, but care must
298 be taken not to saturate the filters or gas concentrations and ratios will not be
299 representative. Saturation can be avoided using bubblers, which involves pumping
300 plume gas through glass flasks with a fritted tip submerged in an absorbing
301 solution. The Rashig tube (involving pumping gas through a rotating glass tube
302 filled with glass rings and an absorbing solution) and denuders (glass tubes coated

303   with an interior coating of reactive compounds, through which gas is pumped to
304   sample reactive halogen species) have also recently been used.

305   The most-commonly used method for real-time in-plume measurements is the
306   Multi-GAS. In Multi-GAS instruments, the air-diluted volcanic gas is passed
307   through a series of electrochemical and/or non-dispersive infrared (NDIR) sensors.
308   Each sensor measures the concentration of a target gas species in the mixture.
309   The number and specificity of sensors used varies greatly between Multi-GAS
310   designs. CO_2 is typically measured by an NDIR sensor, H_2O by an NDIR or derived
311   from a relative humidity sensor, while SO_2, H_2S, CO and H_2 are typically measured
312   by specific electrochemical sensors (H_2 can also be measured by a semi-
313   conductor sensor). Br and Cl electrochemical sensors have also been tested with
314   mixed results so far. All sensors must be calibrated for response (and cross
315   sensitivity) prior to use in the field, and frequent re-calibration of the permanent
316   instrument is required to correct for any drift. Each sensor has a specific calibration
317   range and care must be taken not to oversaturate it. Since its first deployment, the
318   Multi-GAS has quickly become the most widely used instrument for measuring the
319   chemical composition of volcanic plumes, both during campaign measurements
320   and in permanent deployments. The main advantages of the system are its
321   robustness, low cost, near real-time results, and its ability to acquire data
322   autonomously at a frequency of 1Hz. The Multi-GAS technique is particularly well
323   suited for permanent installations. Dozens of active volcanoes currently have
324   permanent Multi-GAS units monitoring the composition of their volcanic gases in
325   real time.

326   Both the filter pack and the Multi-GAS instrument provide ppmv concentrations of
327   gas species, which are then converted into molar ratios. The ratio of all species to
328   a common denominator allows the complete gas composition to be determined.
329   Volcanic gas composition is a complex function of (1) parent melt composition and
330   volatile content, (2) exsolution and gas separation depth/pressure, (3)
331   temperature, (4) oxidation state, and (5) hydrothermal interactions. Changes in
332   volcanic gas composition over time have therefore been related to changes in any
333   one or a combination of these parameters and have now been observed at multiple
334   volcanoes both during and prior to eruption.

335   *Case study box: Turrialba*

336   A remarkable example of how fumarole (direct sampling) and plume (Multi-GAS)
337   monitoring can integrate to capture activity escalation in the run-up to eruption has
338   recently been offered by Turrialba (Costa Rica). Geochemical monitoring of
339   Turrialba over the last quarter century has documented a spectacular transition
340   from hydrothermal to magmatic gas compositions preceding phreatomagmatic to
341   magmatic eruptions (Figure 4). This monitoring period also spanned the
342   technological advent of the Multi-GAS. Prior the mid 1990s Turrialba had been
343   dormant for almost one and half centuries, and the reactivation of the magmatic
344   system occurred slowly, allowing an unprecedented characterization of the
345   changes in gas emissions that are expected at any volcano where a hydrothermal
346   system is displaced by magma emplacement preceding an eruptive period.

347 Direct sampling of the West crater fumaroles between 1998 and 2008 [13] showed
348 gradual and unequivocal changes in gas compositions from hydrothermal to
349 magmatic signatures. Hydrothermal gases were characterized by CO_2/S_t (where S
350 total = H_2S + SO_2) > 100, H_2S/S_t = 1 and very low halogen contents. CO_2/S_t
351 reached a peak in late 2001 early 2002, the first indication of deep magma
352 injection, marking the beginning of radical changes toward magmatic gas
353 compositions. By 2007-2008, the CO_2/S_t ratio had dropped by 3 orders of
354 magnitude, H_2S/S_t had decreased to essentially zero, and $(HCl+HF)/CO_2$ had
355 increased by >2 orders of magnitude. By this time, small vent-opening eruptions
356 occurred in 2010, 2012 & 2013, making direct sampling of the fumaroles in the
357 west crater too dangerous.

358 A Multi-GAS station was installed at the summit in early 2014, just in time to record
359 changes in the plume gases prior to the violent phreatic eruption of October 2014
360 and the subsequent progression into phreatomagmatic eruptive activity in 2015
361 [18]. Clear peaks in CO_2/S_t were observed in the weeks preceding the first three
362 eruptive phases (black stars Figure 4), indicating that deep magma injection was
363 driving the activity. The baseline H_2S/S_t ratio prior to and between the initial
364 eruptive episodes was ~0.5, higher than that observed in the highest temperature
365 fumaroles of the West crater in 2008, and consistent with the idea that the Multi-
366 GAS was measuring bulk gas emissions from diverse fumarolic/vent sources
367 within the crater. From mid-2014 to late 2015 the H_2S/S_t and CO_2/SO_2 ratios varied
368 wildly, indicating instability of the system and expulsion of the hydrothermal system
369 by intruding magma (period A, Figure 4).

370 The process of vent opening and displacement of the hydrothermal was completed
371 by early 2016, and gas compositions changed abruptly to purely shallow magmatic
372 in character, with CO_2/S_t < 5 and H_2S/S_t < 0.1 (period B, Figure 4). The summit
373 Multi-GAS site was no longer sustainable, and a station was installed on the lower
374 flank. Eruptive activity gradually transitioned from violent explosions to dominantly
375 open-vent ash emissions, and in late 2016 and early 2017 small magmatic
376 Strombolian eruptions started occurring, continuing until late 2018. As activity
377 waned in 2019-2020, H_2S/S_t and CO_2/S_t rose significantly, indicating the initiation
378 of the re-establishment of the hydrothermal system (period C, Figure 4).

379 3.3. Ground-based remote plume measurements

380 Remote sensing, wherein absorption of radiation at specific wavelengths by
381 volcanic gases of interest is leveraged in lieu of directly measuring or sampling
382 gas, is a crucial modern subdiscipline of volcanic gas monitoring. In addition to
383 providing data not obtainable by direct measurements (e.g., gas flux), remote
384 sensing measurements also offer safer opportunities for volcanologists to measure
385 magmatic gas compositions and fluxes in real time even during violent eruptive
386 activities.

387 Many of the major volcanic gas species have absorption features in the ultraviolet
388 (UV) and/or infrared (IR) parts of the electromagnetic spectrum that are sufficiently
389 distinct to be resolved by remote sensing [1,6,7]. SO_2 has strong absorption

390 features in both the UV and IR, and its negligible (ppb) levels in the background
391 atmosphere make it the easiest volcanic gas to measure by ground-based remote
392 sensing. H_2O, CO_2, CO, HCl, HF, SiF_4, and OCS all have absorption features in
393 the IR and have been measured using open-path Fourier transform infrared (OP-
394 FTIR) spectrometers. Isolation of volcanic H_2O and CO_2 signals from the
395 atmospheric background can be problematic but can be achieved by using their
396 concentration ratio to purely volcanic species (SO_2, HCl). Typically, a hot IR source
397 (the magma itself in most applications) and low ambient air H_2O contents are
398 required. Some attempts have also been made to measure H_2O in the visible and
399 UV ranges. H_2S, despite a shortwave UV absorption feature, is typically difficult to
400 measure unless an active source, such as a UV lamp, is used. H_2 has not been
401 measured by either UV or IR remote sensing so far. HBr itself has also not been
402 measured, but once oxidized to BrO can be measured in the UV.

403 The volcanic SO_2 flux is one of the principal monitoring datasets at many active
404 volcanoes. The amount of SO_2 emitted is inextricably linked to the type of volcano
405 and how it behaves [1], and, in many cases, SO_2 fluxes can be used as a rough
406 proxy for eruptive activity levels.

407 Ground-based SO_2 flux measurements most often utilize UV differential optical
408 absorption spectroscopy (DOAS), either via a single spectrometer, a network of
409 multiple spectrometers, or integrated into a SO_2 camera. In either cases, the
410 amount of gas between the spectrometer and the radiation source is derived via
411 the Beer-Lambert law. Single-spectrometer measurements are inherently limited
412 in temporal resolution, given the finite time necessary to complete a scan or
413 traverse (every few minutes at best), which can limit integration with data of higher
414 temporal resolution (e.g., seismicity or infrasound). The resolution of SO_2 flux
415 datasets can be improved, however, by utilizing spectrometers in other
416 configurations. Networks of scanning or static upward-looking spectrometers offer
417 SO_2 flux measurements at up to ~1 Hz. Similarly, spectrometer-integrated SO_2
418 camera also offers high-resolution of SO_2 fluxes, but with the added benefit of a
419 synoptic view of plume behavior, which provides important context for interpreting
420 degassing dynamics. High spatial resolution allows resolving emissions from
421 individual vents.

422 OP-FTIR spectroscopy provides information on additional gas species using
423 natural IR sources, such as lava or the sun, or active sources, such as IR lamps.
424 If the path-length is known, average gas concentrations may be calculated; often,
425 results are instead presented as molar ratios of gas species. Measurements made
426 via OP-FTIR have been utilized at high temporal resolution (up to 1 Hz) to
427 investigate rapid, short-term changes in gas chemistry correlated with rapid
428 changes in eruptive dynamisms [18], as well as with geophysical signals. They can
429 also be used to monitor plume degassing at open-vent volcanoes over longer
430 periods. Ratios of different gas species to SO_2 can be leveraged alongside
431 independently measured SO_2 fluxes to quantify the of each gas species and bulk
432 gas fluxes. The wide range of gases that can be measured via OP-FTIR includes
433 a number of redox couples (e.g., CO_2/CO) that can also provide information on
434 changing redox conditions and degassing style.

Case study box: Cotopaxi and Kīlauea.

436 Often, as dormant or quiescent volcanoes begin to build toward renewed activity,
437 one of the quantifiable manifestations of the reawakening is an increase in SO_2
438 emissions. This has been documented for many eruptions, including Pinatubo
439 (Philippines, 1991), Mount St. Helens (USA, 2004), Redoubt Volcano (USA, 2009),
440 and others. More recently, the 2015 eruption of Cotopaxi (Ecuador) – the first since
441 the 1940s – exhibited a precursory increase in SO_2 emission as detected by their
442 network of scanning DOAS spectrometers [19]. Since 2008, the two permanent
443 DOAS scanners have measured SO_2 fluxes with a temporal resolution of ~10
444 minutes. Beginning in mid-May of 2015, ~6 weeks after an initial increase in
445 seismicity, SO_2 emissions began to climb from ~30 to ~300 t/d. From the end of
446 May through the onset of explosive eruptions in mid-August, SO_2 emissions
447 increased further and varied between a few hundred and a few thousand t/d. BrO
448 was detected beginning in June as discrete seismic events began to transition to
449 tremor, and HCl was detectable by FTIR by early August. During the months-long
450 eruptive period from August through November, SO_2 emissions were still higher,
451 averaging ~3,000 t/d, with individual measurements up to ~25,000 t/d. The
452 precursory sequence of combined seismic and gas data was interpreted to be the
453 manifestation first of shallowing magma that was still deep enough to inhibit most
454 sulfur exsolution, followed by further shallowing of the magma, which brought
455 about the onset of enhanced sulfur degassing and measurable halogen degassing.

456 While the Cotopaxi eruption is an example of increasing SO_2 emissions during
457 precursory unrest after decades of quiescence, a number of volcanoes also show
458 the opposite. A decrease in SO_2 emissions ahead of explosive activity, a sign of
459 sealing and pressurization, on timescales of minutes to days or weeks – as
460 measured by SO_2 camera or DOAS network – has been documented at systems
461 including Fuego (Guatemala), Galeras (Colombia), Popocatépetl (Mexico),
462 Karymsky (Russia), and Sinabung (Indonesia).

463 Though less common at basaltic, non-arc systems – because of the high solubility
464 of sulfur in basalt [4] that typically limits sulfur degassing to very near-surface
465 (≲500 m) – changes in SO_2 emissions can also sometimes herald changes in
466 eruptive activity at such volcanoes. In late 2007 through early 2008, even as a
467 decades-long rift eruption of Kīlauea (USA) continued, summit SO_2 emissions –
468 measured routinely since the 1970s – began to increase over the course of a few
469 months, from ~200 to ~1500 t/d [20]. There was a concurrent decrease in the
470 CO_2/SO_2 ratio of the summit gases; seismic activity in the summit area increased
471 as well, preceding the onset of the SO_2 increase by ~1 month. Thus, gas and
472 seismicity appeared to hint at potential eruptive activity. There was, however, no
473 shallow (1-2 km) inflation, which would normally be expected in advance of an
474 eruption. To the contrary, a deflationary trend that began more than a year prior
475 continued unchanged. An incandescent fumarole field developed after ~3 months
476 of increasing SO_2 emissions; the vent-clearing explosion, which formed a new
477 crater and marked the onset of a decade-long summit lava lake eruption, took
478 place a week later. In this case, where deformation seemed to indicate otherwise,

479 | the progressively increasing SO_2 emissions indeed were a key precursor to the
480 | new eruption for Kīlauea.

481 3.4. Satellite-based remote plume measurements.

482 Satellite measurements complement ground-based volcanic gas monitoring by
483 covering larger spatial scales (regional to global), ensuring geochemical
484 surveillance of otherwise unmonitored volcanoes, and providing observations
485 when conditions become too hazardous for proximal data collection (e.g., during
486 the precursory phase of major eruptions) [21]. Satellite and ground-based remote
487 sensing of volcanic plumes rely on the same fundamental principles, i.e., observing
488 the absorption of electromagnetic radiation in the UV and IR spectral bands by
489 volcanic gases and using this to quantify atmospheric column amounts of the
490 target gas species. Routine, satellite-based geochemical monitoring of volcanic
491 gases in lower tropospheric plumes (i.e., passive degassing) is currently restricted
492 to SO_2 and possibly BrO [6,21]; a more extensive suite of gas species can
493 potentially be detected in eruptive emissions (e.g., CO_2, CO, HCl, OClO) due to a
494 combination of higher plume altitude, larger gas amounts, and more accessible
495 absorption bands. UV satellite instruments have greater sensitivity to lower
496 tropospheric SO_2 than IR sensors, and so the former are favored for space-based
497 monitoring of volcanic emissions but are limited by the availability of UV radiation.
498 IR sensors provide critical observations during the night and at high latitudes in the
499 winter months.

500 Satellite measurements of volcanic plumes offer several advantages over other
501 monitoring techniques. They provide daily, near-global coverage of volcanic
502 degassing and some satellite missions, in operation since the early 2000s, now
503 provide unique, multi-decadal time series of SO_2 emissions from SVGE volcanoes.
504 Two decades of UV measurements by the Ozone Monitoring Instrument (OMI) on
505 NASA's Aura satellite have permitted the compilation of a comprehensive
506 inventory of ~100 SVGE volcanoes characterized by persistent SO_2 emissions
507 (Figure 6), providing new constraints on the global volcanic SO_2 flux and on the
508 fluxes of other volcanic gases (e.g., CO_2) when combined with in-situ
509 measurements of gas ratios. The OMI SO_2 inventory (Figure 6), now being
510 integrated with results from the more recent TROPOMI, provides a snapshot of
511 global volcanic degassing, including persistent, high SO_2 fluxes from many open-
512 vent SVGEs (e.g., Etna, Manam, Popocatepetl), some abrupt changes in SO_2
513 emissions at SVGEs that host basaltic lava lakes (e.g., Ambrym, Kīlauea,
514 Nyiragongo), and notable recent trends toward higher SO_2 emissions at some
515 volcanoes (e.g., Sangay, Sabancaya). In addition to detecting any significant
516 changes in SO_2 flux at SVGEs, satellites also permit rapid identification of any new
517 SO_2 emissions (above detection limits, which may be on the order of 100s of t/d
518 SO_2 or more) from previously inactive volcanoes, such as WVGE volcanoes in
519 transition to a more active state. Such data can be used to assess the need for
520 increased geochemical surveillance via deployment of ground-based
521 instrumentation. Unlike many ground-based UV spectrometer networks at
522 degassing volcanoes, satellite-based detection of volcanic SO_2 plumes is
523 insensitive to wind direction. Furthermore, all satellite data from a given sensor are

524 processed using the same SO_2 retrieval algorithm, providing a level of consistency
525 (and the opportunity for reprocessing as algorithms improve) lacking in ground-
526 based remote sensing data collected using a variety of instruments.

527 Disadvantages of satellite observations include lower sensitivity to volcanic SO_2
528 than ground-based measurements, a reliance on relatively clear observing
529 conditions (meteorological clouds often partly or completely obscure volcanic
530 plumes at lower altitudes), and relatively low temporal resolution. The satellite orbit
531 governs the temporal resolution of the measurements, and most UV and IR
532 sensors measuring volcanic SO_2 operate in polar orbit, typically providing data only
533 once or twice per day at low latitudes. However, over the coming decade a new
534 constellation of geostationary UV satellite sensors will provide hourly SO_2
535 measurements in daytime for some volcanic regions (North America, Europe and
536 East Asia). Satellite measurements of SO_2 are also typically reported as SO_2 mass
537 rather than SO_2 flux, in contrast to ground-based SO_2 data, hence merging the two
538 datasets can be challenging. Various techniques are being refined for estimating
539 SO_2 fluxes from satellite observations.
540

541 *Case study box: Fourpeaked Mountain and Merapi*

542

543 Timely detection of new SO_2 emissions at reawakening, unmonitored volcanoes is
544 critical, as it can be diagnostic of magmatic intrusions that may progress toward
545 eruption, prompting a major reassessment of potential volcanic hazards. Long-
546 dormant volcanoes (e.g., WVGEs) typically host extensive hydrothermal systems
547 that may initially scrub SO_2 before the hydrothermal fluids dry out and SO_2
548 emissions increase. In September 2006, ice-clad Fourpeaked Mountain (USA),
549 thought to have been inactive in the Holocene, produced an ostensibly phreatic
550 eruption that nevertheless emitted SO_2 (~2000 tons) clearly detected from space
551 by Aura/OMI. This satellite data and other observations prompted increased
552 surveillance of Fourpeaked Mountain by the U.S. Geological Survey Alaska
553 Volcano Observatory (USGS/AVO), including the installation of a seismic network
554 and further airborne volcanic gas measurements. Fourpeaked Mountain now ranks
555 as an historically active volcano, despite not appearing on the list prior to 2006.
556 Similar, potentially 'vanguard' SO_2 emissions were detected by Aura/OMI at
557 Garbuna volcano (Papua New Guinea) in October 2005; the first known historical
558 eruption from a volcano whose last major eruption was about 1800 years ago.

559

560 The significance of these small but measurable SO_2 emissions is not yet fully
561 understood, although activity at Fourpeaked Mountain has been ascribed to a
562 shallow magmatic intrusion that stalled, cooled, and degassed in the upper 10 km
563 of the crust. It has been suggested that the discharge of >100 t/d SO_2 should be
564 regarded as diagnostic of magma intrusion, rather than the expulsion of gas from
565 pressurized hydrothermal systems, since SO_2 is not easily extracted from
566 hydrothermal fluids. Small SO_2 emission events without significant discharge of
567 juvenile magma could be regarded as 'failed eruptions' and may be common in the
568 life cycle of a volcano, but it is only very recently (the last two decades) that satellite
569 observations capable of detecting such events have become available.
570

571 Satellite measurements also enable detection of significant changes in SO_2
572 emissions at active volcanoes. Prior to major explosive eruptions, conditions can
573 become challenging for ground-based remote sensing (e.g., due to destroyed
574 equipment; extensive, ash-laden plumes; or evacuations preventing access to
575 instruments and/or roads), or increasingly vigorous emissions may drift beyond the
576 range of ground-based spectrometer networks. During precursory unrest before
577 the major November 2010 eruption of Merapi volcano (Indonesia), satellites played
578 a key role in monitoring increased SO_2 emissions [22]. In late October 2010,
579 seismicity at Merapi increased and a time series of SO_2 emissions derived from
580 satellite measurements showed fluxes greatly exceeding both background and
581 eruptive emissions recorded at Merapi between 1986 and 2007, indicating the
582 ascent of fresh, mafic magma in advance of the paroxysmal phase of the eruption
583 on November 4, 2010. SO_2 emissions temporarily declined to a relatively low level
584 (but still at elevated levels relative to previous Merapi eruptions) during the growth
585 of a lava dome on November 1-3, 2010, but ramped up again significantly on
586 November 3, and peaked during the climactic explosive eruptions of November 4-
587 5.

588 3.5. Soil degassing

589 At closed-vent volcanoes, the largest fraction of the magmatic volatile output is not
590 sustained by crater fumaroles/plumes, but rather by more "invisible" diffuse
591 emissions from degassing soils. Soil degassing from volcano summits, flanks and
592 peripheries hence represents a sensible tool to monitor changes in volcanic
593 activity. CO_2 is the main soil gas constituent, and monitoring the soil CO_2 flux
594 contributes to understanding volcano behavior and state.

595 The soil CO_2 flux is the result of two different processes [23]: diffusion and
596 advection. Molecular diffusion is the process in which gas is transported from a
597 region of high concentration to a region of low concentration. Advection is the
598 process where gas is transported in response to a pressure gradient. Gas transport
599 occurs by a combination of these two processes and the total flux is the sum of the
600 advective and diffusive components. Generally, low CO_2 fluxes are associated with
601 diffusion, whereas high values occur when advection is the prevalent gas transport
602 mechanism. Soil degassing is typically structurally controlled, with fractures and
603 faults acting as main pathways of gas transport and surface release. Mapping of
604 soil CO_2 emissions at volcano-scale is hence a convenient method for identifying
605 structural lineaments and faults related to the regional or local tectonic setting.

606 The soil CO_2 flux is typically measured by the accumulation chamber method,
607 which uses the temporal dependence of CO_2 concentration inside a closed
608 chamber placed above the ground to calculate a flux [23]. The accumulation
609 chamber can be applied either (i) during periodic soil surveys, in which
610 measurements are carried along a regular grid to identify anomalously degassing
611 Diffuse Degassing Structures (DDS) and hence measure their total CO_2 flux (in
612 units of tons/d) or (2) by fully automated, permeant instrument measuring in near
613 real-time the site-specific CO_2 flux (expressed in $g\ m^{-2}\ d^{-1}$), and its changes through

614   time. While (i) is especially useful for mapping, and for reconstructing volatile
615   output budgets, methodology (ii) is especially useful for volcano monitoring.

616   *Case study box: Stromboli and El Hierro*

617   Continuous accumulation chamber measurements have proven especially useful
618   for capturing escalating soil CO_2 fluxes in the run-up to eruption. At Stromboli, an
619   open-vent volcano in the Aeolian archipelago (Italy), persistent mild (Strombolian)
620   explosive activity is occasionally interrupted by potentially tsunamigenic explosive
621   (paroxysmal) and effusive eruptions, the most recent of which occurred in 2002-
622   2003, 2007, 2014, and 2019. Continuous soil CO_2 fluxes, acquired since 1999 with
623   automatic accumulation chambers on the volcano's summit, have been especially
624   useful to characterize, and eventually forecast, the Strombolian-to-effusive activity
625   transition [24] (Fig. 7a). The volcano's CO_2 output is modulated by a delicate
626   dynamic balance between the rate of magma supply and degassing in the
627   plumbing system, and the rate of CO_2 surface release from the plume, soils, and
628   thermal aquifer (Fig. 7b). Increasing CO_2 flux is a hint for escalating CO_2 supply
629   from ascending, volatile-rich magma. Elevated CO_2 fluxes (up to 30,000 g m^{-2} d^{-1})
630   were repeatedly observed prior to effusive eruptions in 2002-2003, 2007, and 2014
631   (Fig. 7b). Also, CO_2 fluxes progressively increased from 2005 to 2019, at an
632   average rate of 4.1 g m^{-2} d^{-1}, and even more substantially (at a rate of 24.2 g m$^-$
633   ^{2}d^{-1}) since 2016. Very high fluxes, up to 24,000 gm^{-2}d^{-1}, were again detected in the
634   months prior paroxysmal activity in July 2019.

635   CO_2 flux surveys in anomalous areas (and total CO_2 flux quantifications) can also
636   be useful for monitoring purposes. For example, more than 17,000 diffuse CO_2 flux
637   measurements were carried out [25] before and during the 2011-2012 volcanic
638   eruption of El Hierro, the smallest and south-westernmost island of the Canarian
639   archipelago. Two significant CO_2 flux increases were recorded, during the pre-
640   eruptive and eruptive phases, respectively. The first CO_2 flux increase was
641   recorded two weeks before the onset of the submarine eruption (time set at 0 in
642   Figure 7c) with an estimated average CO_2 output (627 t d^{-1}) well above the
643   background (422 t d^{-1}). This increase was likely due to the precursory release of
644   CO_2-rich magmatic gases, sourced by deeply rising magma. The second increase
645   started coincident with the most energetic syn-eruptive seismic activity (see Figure
646   7c) interpreted to reflect relaxation around the magma reservoir that fed the
647   eruption.

648   3.6 Volcanic lakes

649   Many closed-vent volcanoes are topped by colorful crater lakes that, when present,
650   are a primary target of geochemical monitoring. Volcanic lakes [26] are surface
651   manifestations of complex processes occurring in the hydrothermal-magmatic
652   system. Lake chemistry results from a combination of volcanic gas injection, water-
653   rock interaction, dilution by meteoric water, evaporation/degassing, mineral
654   precipitation, drainage and recirculation of water from the lake into the underneath
655   hydrothermal system. Hence, the physical (e.g., volume, temperature) and
656   chemical characteristics (pH, compositions of dissolved, exsolved, and

657 precipitated constituents) of these lakes are variable because they reflect changes
658 in both the sub-limnic hydrothermal system and the feeding magma source. Hyper-
659 acid (pH< 1) hydrothermal fluids [27] can dissolve large quantities of fresh volcanic
660 rock, creating porosity and permeability in the central up-flow zone, whereas
661 secondary mineral precipitation seals fractures where fluid cooling and fluid-rock
662 neutralization reactions take place. In acidic water (pH < 4), CO_2 can pass through
663 crater lakes with minimal interaction (e.g., without being absorbed), whereas at
664 high pH a large fraction of the magmatic CO_2 input can dissolve into water as
665 HCO_3^-. Acidic magmatic gases, such as SO_2, HCl, and HF, are soluble in water
666 and are absorbed in hydrothermal systems and/or volcanic lakes [15]; however, at
667 hyperacidic lake conditions (pH < 1), associated with systems with high magmatic
668 gas inputs, acidic gas species can also pass through the lake. Ultimately, gas
669 fluxes from volcanic lakes depend on the balance between the magmatic gas input,
670 and the capacity of the hydrothermal and limnic systems to absorb them. This
671 balance is predominantly controlled by the volume of lake water relative to the
672 magmatic gas influx, by the solubility of the gas species in question, and pH.
673 Degassing through the surface of a volcanic lake occurs by bubbling
674 (convective/advective degassing), evaporation and diffusion through the water/air
675 interface.

676 Monitoring of lake level/volume, pH, temperature, dissolved components as well
677 the lake gas emissions are effective ways of tracking changes in the hydrothermal-
678 magmatic system. Injection of fresh magmatic fluids can trigger phreatic or
679 phreatomagmatic eruptions, and is typically associated with increasing
680 temperature, loss of lake volume, decrease in pH, increasing degassing of CO_2
681 and acid gases, and increasing concentrations of dissolved components in the
682 lake, especially those derived from fresh intruding magma (such as Mg and rare
683 earth elements). Hydrothermal sealing of the conduit, on the other hand, is driven
684 by secondary mineral precipitation and decreased permeability, and can lead to
685 gas accumulation and pressurization beneath the seal, potentially priming the
686 system for larger eruptions once the seal fails catastrophically.

687 We summarize two distinct scenarios (Fig. 8) for the expected sequence of
688 geochemical signals observable in the run-up to eruption at hyper-acidic crater
689 lakes:

690   1. Eruption after a slow heating of the system due to magma injection. In this
691   scenario, the crater lake system undergoes a gradual transformation. As
692   magma infiltrates the subsurface, temperatures rise slowly, leading to
693   subtle changes in the hydrothermal system. Over time, the lake's water
694   temperature elevates until it evaporates. The injection of a fresh magma
695   drives the Mg/Cl up (because of increased leaching of fresh magma) and
696   increases the SO_2 flux (this increases further once the lake disappears).
697   Initially, the lake plume CO_2/SO_2 ratio increases due to the deep magma
698   recharge initiating the process and then decreases as the magma gets
699   shallower. A further CO_2/SO_2 drop occurs at the time of the eruption as
700   magma remobilizes S from the sublimnic alteration zone (Figure 8).

701   2. Sudden eruption triggered by failure of a hydrothermal seal. In this
702   scenario, the crater lake system experiences a rapid and dynamic shift.
703   Hydrothermal sealing causes pressure to accumulate and temperature to
704   decrease. Temperature then increases once the eruption breaks the seal,
705   and then the lake evaporates completely. Mg/Cl ratio remains constant until
706   the seal breaks, which releases deeper Mg-rich fluids, and Mg/Cl further
707   increases as the lake evaporates (and HCl is lost to the gas plume). SO_2
708   flux decreases as sealing occurs, then SO_2 flux increases moderately as
709   the accumulated SO_2 is released. CO_2/SO_2 increases with sealing, then
710   drops to shallow magmatic values as the seal breaks, and then goes back
711   to background values (Figure 8).

712 The two scenarios above imply that a combination of regular surveys (for crater
713 lake water sampling and analysis) and continuous observations with permanent
714 instrumental networks (DOAS for SO_2 flux and Multi-GAS for plume chemistry) is
715 critically required for effective lake monitoring.

716   4. A general, integrated model for volcano geochemical monitoring.

717 We synthesize the above information, and the results of monitoring efforts in
718 response to recent volcanic unrests/eruptions, in the general model of Figure 9.
719 The figure illustrates, in a simplistic, schematic and hence purely illustrative form,
720 the expected sequence of geochemical changes, and the consequent progression
721 in geochemical monitoring actions, during volcano evolution from dormancy to
722 eruption.

723 During the repose periods of quiescent volcanoes (Fig. 9a), surface gas consists
724 of H_2O-rich hydrothermal vapors. These WSGE emit no SO_2 and HCl, implying that
725 ground-based remote sensing units (e.g., scanning DOAS, SO_2-camera and
726 FTIR), and satellites, will detect no gas at all (Fig. 9a''). In this context, periodic
727 (monthly-to-yearly) direct gas sampling of fumaroles is the most effective
728 monitoring strategy (Fig. 9a). Any summit crater lake will also need to be sampled
729 periodically, to test for temporal stability of temperature, salinity, and compositions.
730 Attempts to measure the fumarolic CO_2 flux will be complicated by the absence of
731 SO_2, and will therefore require profiling CO_2 concentrations in the plume via either
732 ground or airborne surveys. Notably, in such closed-vent volcanoes, this fumarolic
733 CO_2 flux (Fig. 9a'') is normally far more modest than the diffuse CO_2 output from
734 the volcano's flank/periphery, implying that soil CO_2 monitoring is also critically
735 important. During repose, this soil CO_2 output will be dominated by biogenic
736 sources (soil respiration) and will likely exhibit strong seasonal modulations (Fig.
737 9a'').

738 Unrest (Fig. 9b) is typically initiated by an escalating supply of magmatic gases
739 into the hydrologic/hydrothermal system. At this stage, the critical question is to
740 establish if magmatic gases are supplied by decompressing (ascending) mafic
741 magma at depth (magmatic unrest; Fig. 9c), or if instead magma is stationary and
742 releasing volatiles due to crystallization/second boiling. In such a second case,
743 timing and magnitude (flux) of magmatic volatile release at surface will be primarily
744 modulated by pressure build-up underneath (and failure of) a hydrothermal seal

745 (hydrothermal unrest, Fig. 1c). Independent (geophysical) evidence is normally
746 required to resolve the two scenarios, because geochemical data alone provide
747 ambiguous results. Whatever the case, unrest can be tracked by crater fumaroles
748 becoming hotter and more magmatic in nature, e.g., with increasing CO_2 and H_2S
749 proportions relative to H_2O (Fig. 9b'). Fumarolic CO_2/CH_4 and CO/CO_2 ratios are
750 also likely to increase as caused by hydrothermal conditions evolving to higher P-
751 T because of the input of hot, oxidized magmatic fluids [12]. At this stage, it
752 becomes increasingly convenient to combine periodic direct sampling surveys with
753 the installation of the first continuous monitoring sensor kits, especially fully
754 automated accumulation chambers that real-time measure the soil CO_2 flux.

755 If magmatic unrest progresses (Fig. 9c), and hydrothermal reactions become less
756 and less intense, magmatic SO_2 can eventually make its way to the surface,
757 causing the fumarolic CO_2/S_t and H_2S/SO_2 ratios to decrease (S_t is total sulfur)
758 (Fig. 9c'), and the SO_2 flux to become detectable from ground (and eventually from
759 satellites) (Fig. 9c''). The soil CO_2 output is also expected to increase (Fig. 9c'')
760 due to escalating magmatic CO_2 transport, and crater lakes are anticipated to
761 warm up, and to become increasingly acidic and saline (lakes may become
762 permeable to gas, and eventually dry-up and disappear when eruption is
763 approaching). As the unrest ramps up, direct sampling becomes increasingly
764 impractical and hazardous, demanding a transition toward instrumental in-situ
765 observations (e.g., the deployment of a fully automated Multi-GAS). Remote
766 sensing techniques (e.g., scanning DOAS, SO_2 camera, and FTIR) also become
767 instrumental to monitoring, with satellites becoming increasingly useful as gas and
768 thermal output intensify.

769 Monitoring activity in the eruption run-up (Fig. 9d) requires careful analysis of data
770 streamed by multi-sensor instrumental geochemical monitoring networks. High
771 CO_2/SO_2 ratios and increasing CO_2 (and perhaps SO_2) fluxes are likely to become
772 detectable prior (weeks to month) eruption onset (Fig. 9d' and 9d''). As the eruption
773 starts (Fig. 9d), the operability of in-situ instruments is often compromised,
774 demanding a combination of FTIR and airborne (drone-based) Multi-GAS
775 measurements (for chemistry). Remote sensing techniques (from both ground and
776 space) emerge as the key operational tool for eruption monitoring, especially to
777 quantify the large syn-eruptive SO_2 (and HCl) fluxes (Fig. 9d').

778 **5. Summary and future directions.**

779 Geochemical volcano monitoring has transformed in the last few decades. By
780 exploiting data streamed in near real-time by instrumental networks, fluid
781 geochemistry is increasingly becoming an operational tool in the hands of
782 volcanologists, volcanic hazard managers, and decision-makers. We have shown
783 that capturing precursory geochemical change prior to eruption can now be
784 achieved with increasing success when a multi-parameter, multi-instrument
785 network is in place (Fig. 2). This network should be progressively refined as the
786 state of the volcano evolves during unrest, making different monitoring strategies
787 more effective, and in the run-up to eruption (Fig. 9).

788 We expect additional transformation in the field in the years to come, inspired by
789 new technological development. There is growing need of increasing the number
790 of gas species (including, for example, HCl, HF, CH_4, and CO) that can be real-
791 time detected by in-situ permanent instruments (e.g., Multi-GAS). These
792 instruments will need to improve in terms of robustness, operational simplicity and
793 reduced costs, and standardized codes for near real-time data acquisition,
794 processing, visualization, and interpretation (for example, assisted by artificial
795 intelligence) will need to be developed, and distributed to volcano observatories
796 worldwide. Barriers to open data sharing still exist and will need to be overcome.
797 Drones, or UAS (unoccupied aircraft systems), have already been employed at
798 many volcanoes for SO_2 flux measurements, Multi-GAS measurements, gas
799 sampling, and water sampling, and more. Given drones' ability to make proximal
800 measurements in hazardous situations and environments while operators remain
801 at a safe distance, we expect further proliferation of innovative UAS-based volcanic
802 gas measurements in coming years. Satellites are today primarily employed for
803 SO_2 in geochemical volcano monitoring, but measuring other critical species for
804 monitoring, especially CO_2, remains extremely desirable, and will potentially
805 become a reality soon as new airborne IR sensors are deployed onboard new
806 generations of satellites.

807 *6.* **References** *(titles from this and previous editions of the EoV do not count for*
808 *the 20 ref. limit)*

809 [1] J. Stix, P. Nadeau, F. Aguilera, M. Burton, A. Chiodi. Volcanic degassing, this
810 volume, Part 3, Chapter 2.8

811 [2] T.A. Jr. Jaggar, Magmatic gases, American Journal of Science, 238, 5, (1940),
812 313–353, doi:10.2475/ ajs.238.5.313.1940.

813 [3] R.B. Symonds, W.I. Rose, G.J.S. Bluth, T.M. Gerlach, Volcanic-gas studies:
814 methods, results, and applications, Rev. Mineral. Geochem. 30 (1994), 1–66.

815 [4] M. Edmonds, A-S Bouvier, E. Hughes, K. Iacovino, K. Roggensack, A. Shahar,
816 Origins of magmatic volatiles and their role in magma ascent and degassing, this
817 volume, Part 1, Chapter 2.2

818 [5] T.P. Fischer, G. Chiodini, Volcanic, magmatic and hydrothermal gases. In
819 Sigurdsson, H., editor, The Encyclopedia of Volcanoes, 2nd edition, chapter 45
820 (2015), 779–797, Academic Press, Amsterdam.

821 [6] C. Oppenheimer, T.P. Fischer, B. Scaillet, Volcanic degassing, in Holland HD,
822 Turekian KK (eds.), Treatise on Geochemistry, The Crust, 2nd edn, (2014), 111–
823 179, Elsevier.

824 [7] M Edmonds, Geochemical monitoring of volcanoes and the mitigation of
825 volcanic gas hazards, In Papale P (ed.) Hazards and Disasters Series, Forecasting
826 and Planning for Volcanic Hazards, Risks, and Disasters, Elsevier, Volume 2,
827 (2021) https://doi.org/10.1016/B978-0-12-818082-2.09995-9

828 [8] A. Aiuppa, C. Caudron, G. Chiodini, S. Ingebritsen, F. Viveiros, Geochemical
829 monitoring of volcanic fluids in the 21st century. In Spica Z. Caudron C. (eds.)

Modern Volcano Monitoring, Advances in Volcanology series, Springer Nature Switzerland AG.

[9] P. Delmelle, J. Stix, Volcanic gases, In: Encyclopedia of Volcanoes, Sigurdsson H (ed) Academic Press, San Diego, (2000), 803-815

[10] J. Stix, H. Gaonach, Gas, plume and thermal monitoring, In Encyclopædia of volcanoes. Edited by Sigurdsson H., Academic Press, (2000), 1141–1164.

[11] R. Corsaro, et al., Linking subsurface processes to surface observations - rocks, gas, deformation, seismicity (including petrology), this volume, Part 1, Chapter 5.4

[12] G. Chiodini, A. Paonita, A. Aiuppa, A. Costa, S. Caliro, P. De Martino, V. Acocella, J. Vandemeulebrouck, Magmas near the critical degassing pressure drive volcanic unrest towards a critical state, Nat. Comm., 7, (2016), 13712.

[13] O. Vaselli, F. Tassi, E. Duarte, E. Fernandez, R.J. Poreda, A.D. Huertas Evolution of fluid geochemistry at the Turrialba volcano (Costa Rica) from 1998 to 2008, Bull Volcanol 72, (2010), 397–410, https:// doi. org/ 10. 1007/ s00445- 009- 0332-4.

[14] Y. Taran, M. Zelenski, Systematics of water isotopic composition and chlorine content in arc-volcanic gases, Geol Soc Spec Publ, 410 (1), (2015), 237-262, DOI: 10.1144/SP410.5

[15] R.B. Symonds, T.M. Gerlach, M. H. Reed, Magmatic gas scrubbing: implications for volcano monitoring, J. Volcanol. Geotherm. Res., 108, (2001), 303–341

[16] M. Agusto, MC. Lamberti, F. Tassi, et al. Eleven-year survey of the magmatic-hydrothermal fluids from Peteroa volcano: identifying precursory signals of the 2018-2019 eruption, Geochemistry, Geophysics, Geosystems, 24-11, (2023), https://doi.org/10.1029/2023GC011064

[17] G.V. Melián, P.A. Hernández, N.M. Pérez, et al., Insights from Fumarole Gas Geochemistry on the Recent Volcanic Unrest of Pico do Fogo, Cape Verde Frontiers in Earth Science, 9, 631190, (2021), doi: 10.3389/feart.2021.631190

[18] J.M. de Moor, et al, Turmoil at Turrialba Volcano (Costa Rica): Degassing and eruptive processes inferred from high-frequency gas monitoring, J Geophys Res: Solid Earth, 121 (8), (2016), 5761-5775, DOI: 10.1002/2016JB013150.

[18] P. Allard, M. Burton, F. Muré, Spectroscopic evidence for a lava fountain driven by previously accumulated magmatic gas, Nature 433, (2005) ,407–410.

[19] S. Hidalgo, J. Battaglia, S. Arellano, et al., Evolution of the 2015 Cotopaxi eruption revealed by combined geochemical and seismic observations. Geochemistry, Geophysics, Geosystems, 19, (2018), 2087–2108. https://doi.org/10.1029/2018GC007514

[20] M. Patrick, T. Orr, D. Swanson, B. Houghton, K. Wooten, L. Desmither, C. Parcheta, D. Fee, Kīlauea's 2008–2018 summit lava lake—Chronology and eruption insights, In Patrick, M., Orr, T., Swanson, D., and Houghton, B., eds., The

871 2008–2018 summit lava lake at Kīlauea Volcano, Hawaiʻi: U.S. Geological Survey
872 Professional Paper 1867, (2021), https://doi.org/10.3133/pp1867A.

873 [21] S.A. Carn, L. Clarisse, A.J. Prata, Multi-decadal satellite measurements of
874 global volcanic degassing Journal of Volcanology and Geothermal Research, 311,
875 (2016), 99-134. DOI: 10.1016/j.jvolgeores.2016.01.002

876 [22] Surono et al., The 2010 explosive eruption of Java's Merapi volcano—A '100-
877 year' event, Journal of Volcanology and Geothermal Research, 241–242, (2012)
878 121-135, https://doi.org/10.1016/j.jvolgeores.2012.06.018

879 [23] G. Chiodini, R. Cioni, M. Guidi, B. Raco, L. Marini, Soil CO_2 flux measurements
880 in volcanic and geothermal areas, Applied Geochemistry, 13 (5), (1998), 543-552.
881 DOI: 10.1016/S0883-2927(97)00076-0

882 [24] S. Inguaggiato, F. Vita, M. Cangemi, C. Inguaggiato, L. Calderone, The
883 monitoring of CO_2 soil degassing as indicator of increasing volcanic activity: The
884 paroxysmal activity at Stromboli volcano in 2019–2021. Geosciences, 11(4),
885 (2021), 169.

886 [25] G. Melián, P.A. Hernández, E. Padrón, N.M. Pérez, J. Barrancos, G. Padilla,
887 S. Dionis, F. Rodríguez, D. Calvo, and D. Nolasco, Spatial and temporal
888 variations of diffuse CO2 degassing at El Hierro volcanic system: Relation to the
889 2011–2012 submarine eruption, J. Geophys. Res. Solid Earth, 119, (2014),
890 6976–6991, doi:10.1002/2014JB01101

891 [26] P. Delmelle, R.W. Henley, A. Bernard, Volcano-Related Lakes, In
892 Sigurdsson, H., editor, The Encyclopedia of Volcanoes, 2nd edition, chapter 45
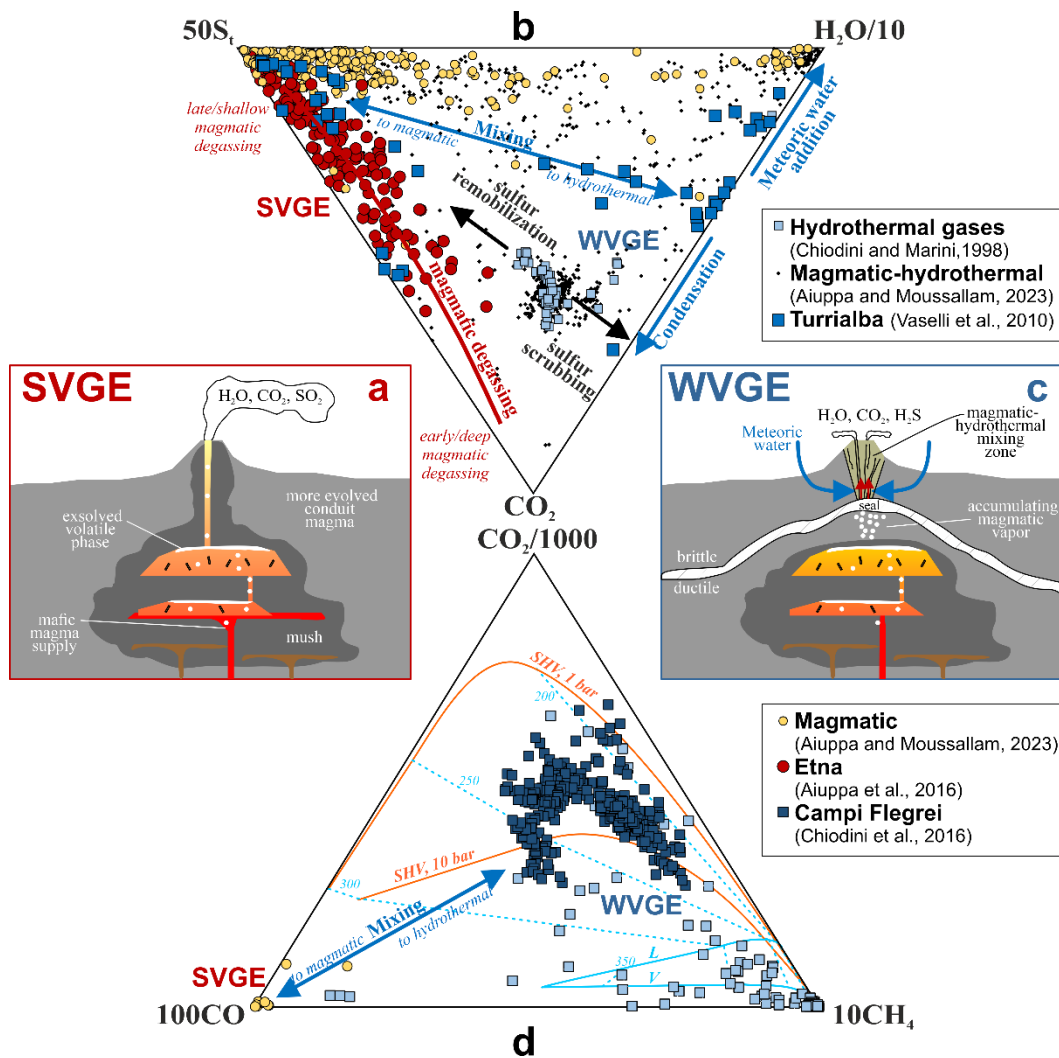893 (2015), 851–864, Academic Press, Amsterdam.

894 [27] H. Shinohara, C. Finn, P. Delmelle, M. Heap, J. Hedenquist, D. Rouwet, B.
895 Scheu, V. Van Hinsberg, Acid altered terrains: Formation, hazards and related
896 uses, this volume, Part 8, Chapter 3.3

897

898 **7. Figure and figure captions.**

899 **Figure 1** – A) A schematic cross-section of a SVGE (Strong Volcanic Gas
900 Emitters) volcano. The magmatic gases they release (by either open-vent
901 degassing or hot dome-hosted fumaroles) are H_2O-CO_2-SO_2 mixtures. In the
902 triangular plot of panel B), these magmatic gases are exemplified by the yellow
903 (data from a global database) and red (Etna) circles. At any given volcano, gas
904 compositional change is controlled by changes in magma degassing depth and
905 extent; see the Etna example (red circles are selected plume results from the
906 Bocca Nuova crater, which range from CO_2-rich deeply exsolved gas to SO_2-rich
907 shallow sourced gas). C) A schematic cross-section of a WVGE (Weak Volcanic
908 Gas Emitters) volcano. Gases are H_2O-CO_2-H_2S mixtures formed by boiling of
909 meteoric water-dominated hydrothermal aquifers, heated by magmatic gases
910 released by magma stored at depth. A hydrothermal mineral seal separates the
911 ductile and brittle crust and modulates (via press-build-up until failure) the rate of
912 magmatic gas supply. At these WVGE volcanoes, the main drivers of chemical

change are temporally variable extents of (i) mixing between magmatic and hydrothermal gases, (ii) sulfur scrubbing in (or remobilization from) hydrothermal minerals/fluids, (iii) steam/condensation, and (iv) meteoric water addition. Hydrothermal to magmatic gas transition is exemplified by the Turrialba gas dataset [13]; D) Relative proportions of C species. Hydrothermal gases from WVGE are CH_4-enriched, and are interpreted to reflect equilibration in the liquid (L), vapor (V) or superheated vapor (SHV) over a range of hydrothermal temperatures (light blue dashed °C). Drivers of change (as exemplified by the Campi Flegrei case) are either changing hydrothermal P-T-X conditions, or mixing with magmatic gases, that are CO-rich and CH_4-poor (often CH_4-free; data from [5]).

926 **Figure 2** – Integrated geochemical monitoring network during A) repose, B)
927 escalating degassing (unrest), C) eruption. Turrialba volcano in background (photo
928 credits, J.M.D.M).
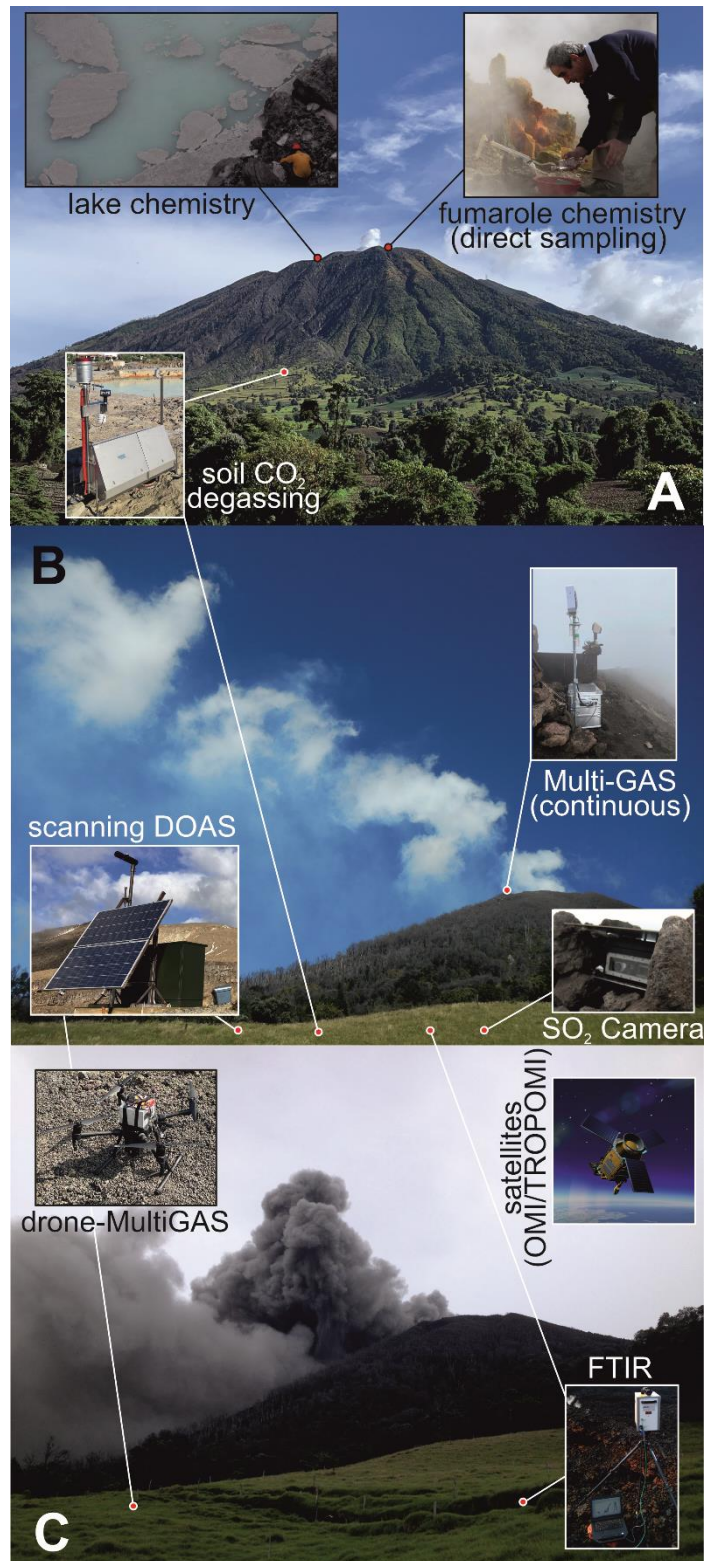
929

930

931 **Figure 3** - a) Peteroa volcano gas time series. The panels illustrate the temporal
932 evolution (2010 to 2021) of SO_2/H_2S, $100*HCl/CO_2$, $1000*HF/CO_2$ (thin dashed
933 lines point out 0.1 ratio values), CH_4/Ar ratios, $^3He/^4He$ (Rc/Ra), and $\delta^{13}C-CO_2$
934 (‰vs. V-PDB) in fumarolic gases [16]. b) Pico do Fogo volcano gas time series.
935 The plot illustrates the temporal evolution (2007 to 2018) of CO/CO_2, H_2/CO_2,
936 $\delta^{13}C-CO_2$ (‰vs. V-PDB), and equilibrium temperature (EqT; estimated based on
937 the $CH_4-CO-CO_2$ system: $3CO_2 + CH_4 \Leftrightarrow 4CO + 2H_2O$) in two fumarolic vents
938 (F1 and F2) [17]. Gray shaded areas highlight phases with magmatic gas
939 signatures. The phreatic, phreato-magmatic, and magmatic eruptions (between
940 thick dashed lines) are also indicated.
941
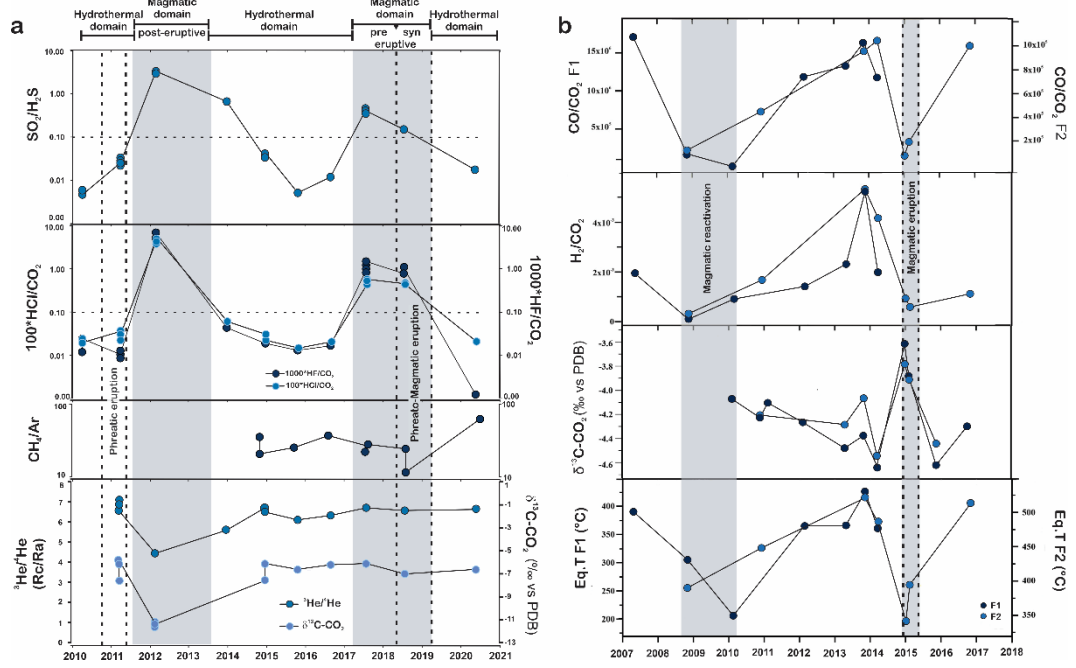
942
943

944   **Figure 4** - Changes in gas compositions at Turrialba volcano from direct sampling
945   (left panels, 1998-2008) and Multi-GAS (right panels, 2014-2020) tracked the
946   displacement of the hydrothermal system by magma intrusion, preceding vent-
947   opening eruptions, years of semi-continuous ash emissions, and small
948   Strombolian eruptions (note a small Multi-GAS data gap in 2019).
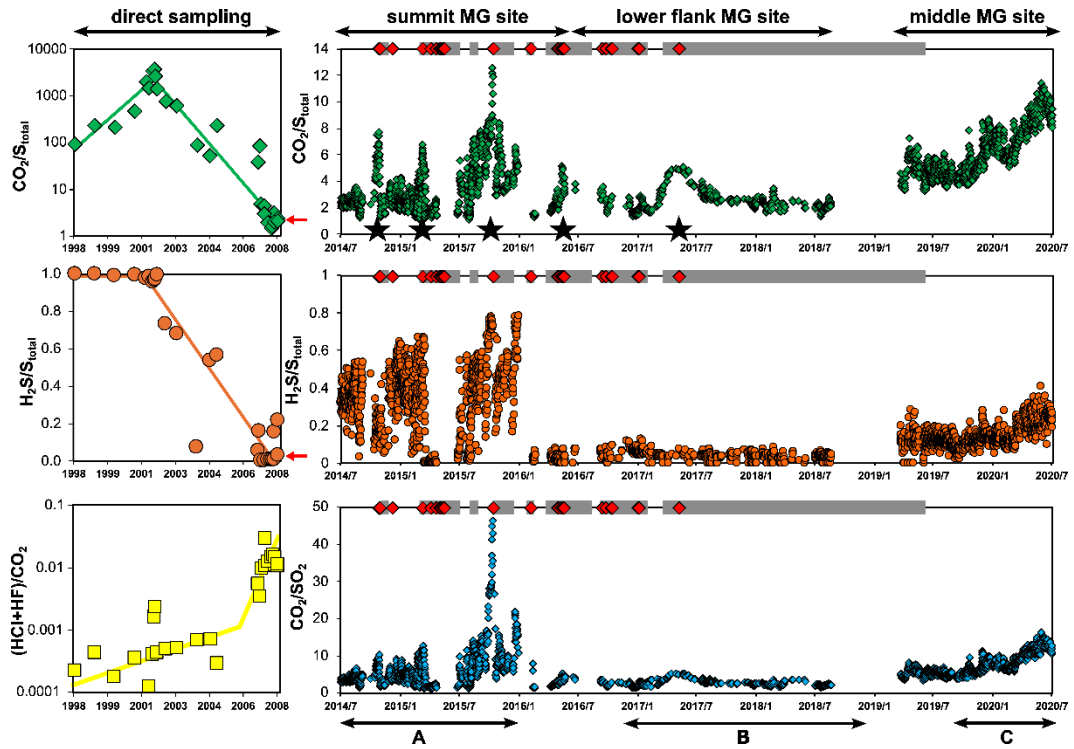
949

950

951 **Figure 5 -** Top: SO_2 emissions (red), transient seismic events per day (gray), and
952 SO_2/HCl ratios (blue) during 2015 at Cotopaxi Volcano. Both seismicity and SO_2
953 emissions began to increase months in advance of the eventual eruptive activity
954 in mid-August, indicating shallowing magma. The detection of HCl in early August
955 further supported the interpretation that magma was nearing the surface. Seismic
956 data courtesy of Silvana Hidalgo. Gas data available at
957 http://dx.doi.org/10.1594/IEDA/111165. Bottom: SO_2 emissions (red), weekly
958 RSAM (station RIM, gray), and GPS North-South displacement (station UWEV,
959 blue) in late 2007 and early 2008 at the summit of Kīlauea. Though GPS indicated
960 continued shallow deflation, both seismic tremor and SO_2 emissions began to
961 climb above background in November and December of 2007, hinting at
962 shallowing magma. A new fumarole field appeared on 12 March 2008 and became
963 incandescent a few days later, less than a week before the onset of the new
964 eruption. Data from ref. [20] references therein.

965

966
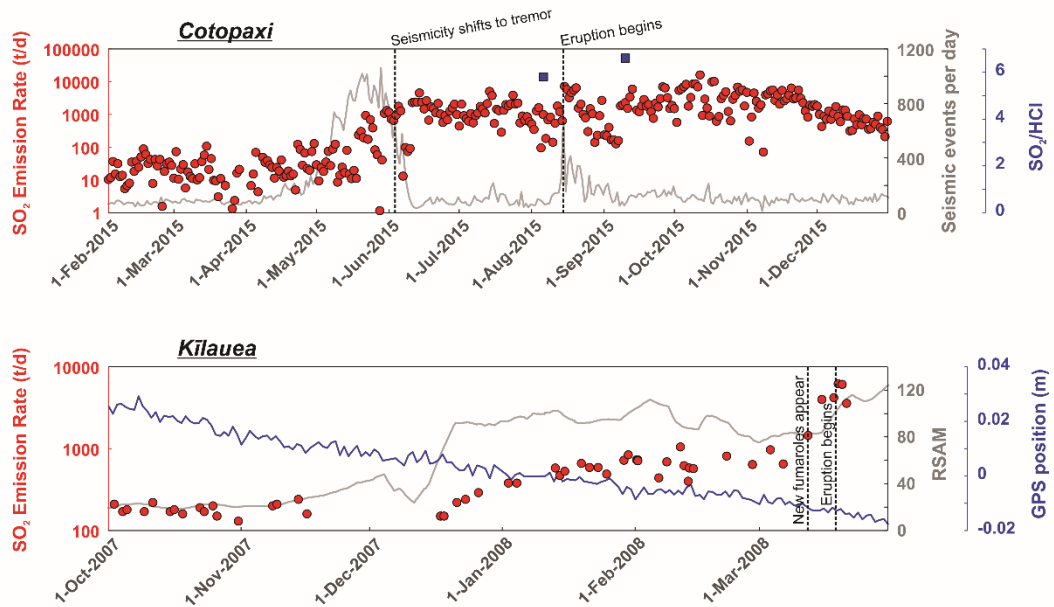
Figure 6 - Time series of annual mean SO$_2$ emissions in 2005-2022 for 104 degassing volcanoes derived from NASA/Aura Ozone Monitoring Instrument (OMI) satellite observations. Each panel shows the SO$_2$ time series for the indicated volcano (white or gray curve) on a log scale (y-axis is scaled from 0.01-20 kilotons/day on each plot), the mean SO$_2$ flux (*horizontal red line*), and the SO$_2$ flux (kt/day) in 2022 (red dot; only shown if >0.01 kt/day). Panels are colored and ordered based on the percentage difference between the SO$_2$ flux in 2022 and the mean SO$_2$ flux.
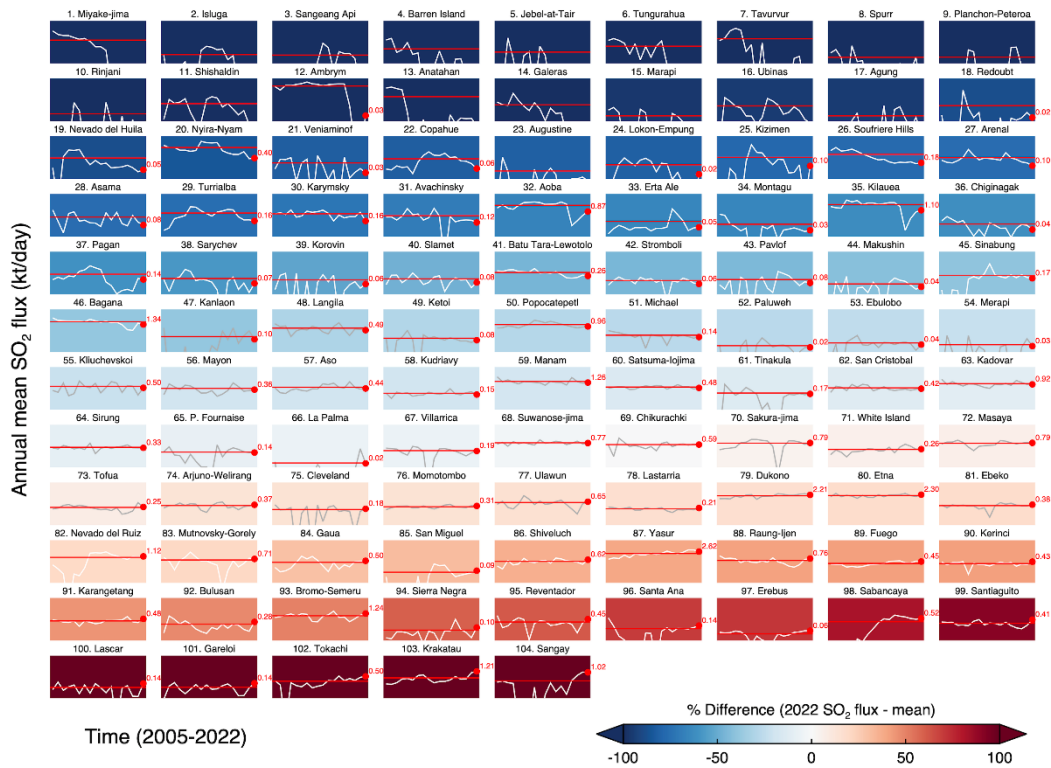
977   **Figure 7**- a) Daily averaged (24 measurements/day) CO_2 fluxes at Stromboli in the
978   2001 to 2018 period. Onset of the 2002–2003, 2007, 2014, and 2019 eruptions are
979   indicated. B) Sketch of the stromboli plumbing system: exsolved volatiles from the
980   degassing magma are primarily emitted by the plume, and partially interact with a
981   summit hydrothermal system to feed cold fumaroles, diffuse soil degassing, and
982   thermal waters. When the dynamic equilibrium between gas input and output is
983   altered by increasing magmatic gas supply from depth, the hydrothermal system
984   releases more CO_2 to the surface; C) Time series of the 24 h moving averages of
985   diffuse CO_2 flux at a fixed station (gray) and temporal evolution of total diffuse CO_2
986   flux (black) during 2011–2012 at El Hierro volcano. Time is expressed in days
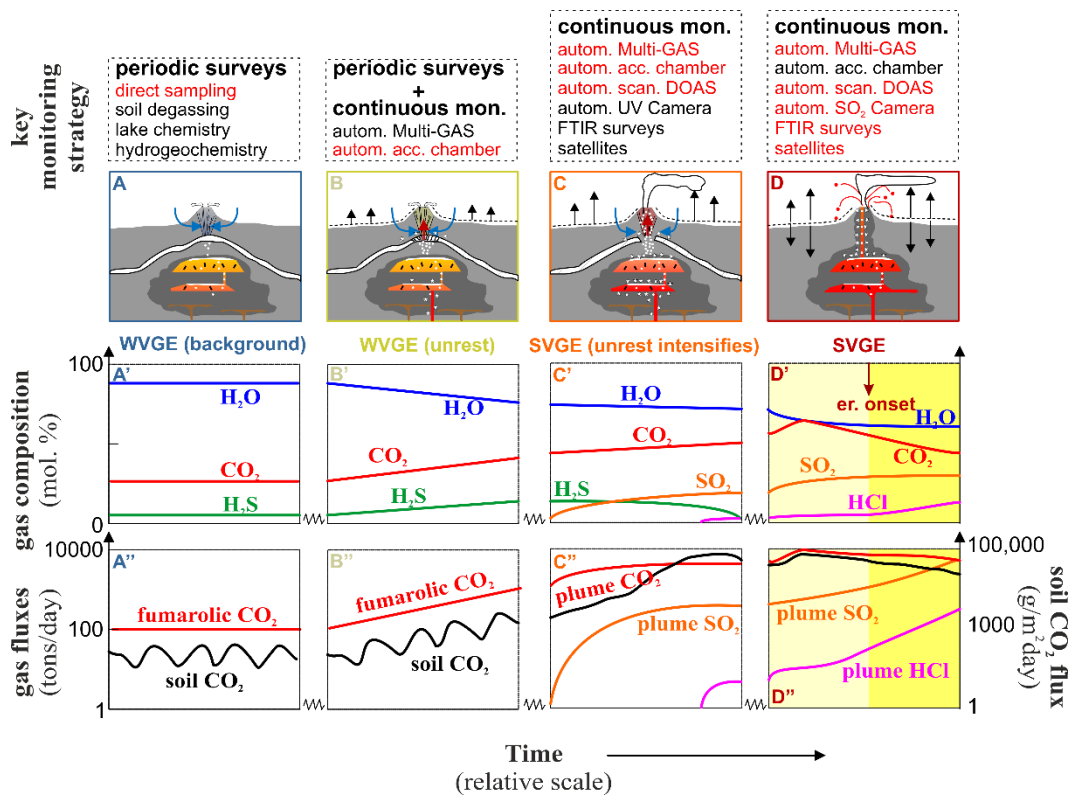987   before/after eruption onset.
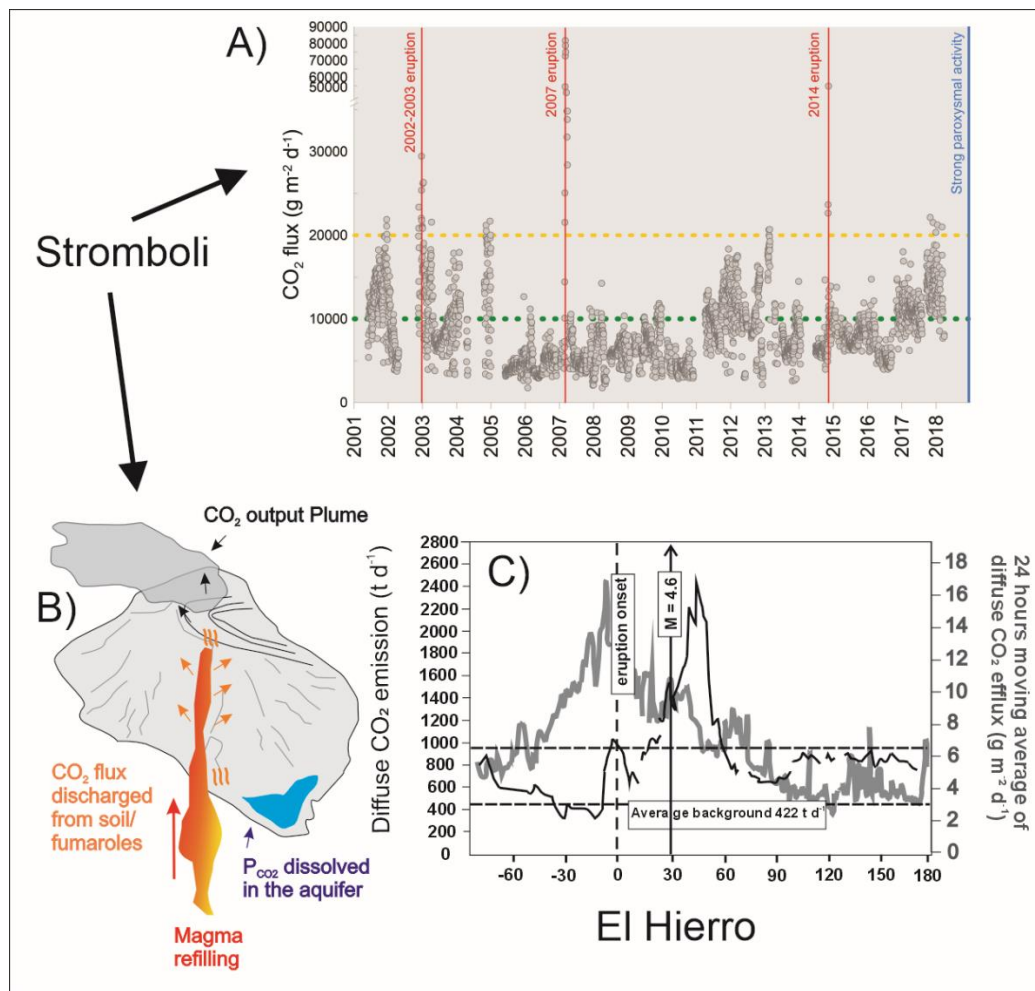
988

989

990 **Figure 8**: (right) Sketch showing the typical structure of a hyper-acid high-activity
991 lake. (Left) Idealized time series illustrate the expected changes for a few key
992 geochemical monitoring parameters for 2 end-member cases: Red lines show the
993 expected progression for the run-up to an eruption driven by deep magma injection
994 and magma rising to the surface, whereas the blue lines show the expected
995 progression for a system that becomes hydrothermally sealed and then erupts due
996 to pressure/volatile accumulation below the seal. The process leading up to
997 eruption starts at t_1, where new magma starts being injected, raising lake
998 temperature (until the lake evaporates at t_3). Fresh rock in the system drives Mg/Cl
999 up, rising magma drives increasing SO_2 degassing (which increases further once
1000 the lake disappears at t_3), initially associated with an increase in CO_2/SO_2 (deep
1001 magma recharge initiating the process) and then decreasing CO_2/SO_2 as the
1002 magma rises (another drop in CO_2/SO_2 occurs at the time of the eruption as
1003 magma remobilizes S from the sublimnic alteration zone). For the case of pressure
1004 accumulation by sealing, the lake temperature decreases, then surges once the
1005 eruption breaks the seal, and then the lake evaporates completely. Mg/Cl stays
1006 constant until the seal breaks, which releases deeper Mg-rich fluids, and Mg/Cl
1007 increases as the lake evaporates. SO_2 flux decreases as sealing occurs, then
1008 comes out moderately as the accumulated SO_2 is released. CO_2/SO_2 increases
1009 with sealing, then drops to shallow magmatic values as the seal breaks, and then
1010 goes back to background values.

1011
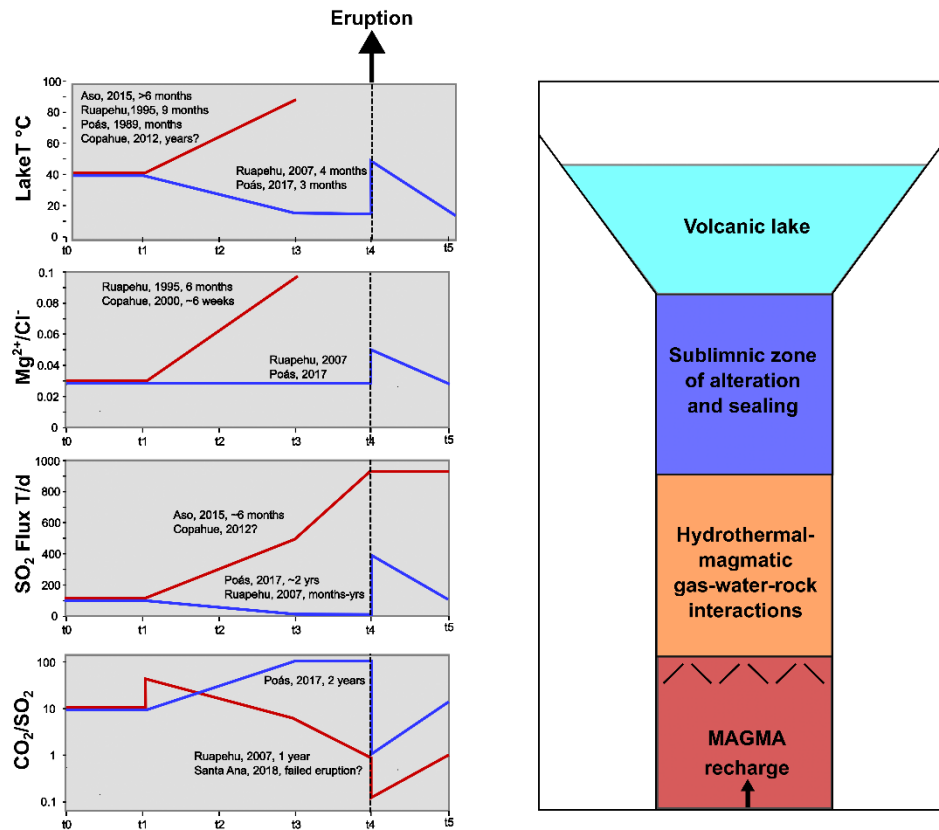
1012 **Figure 9** - A schematic, purely illustrative model describing the expected sequence
1013 of geochemical changes (panels A' to D'') during a hypothetical volcano dormancy-
1014 to-eruption progression. Panels A to D exemplify key processes in the magmatic
1015 plumbing system and in the overlying hydrothermal system. The two are thought
1016 to be separated by a hydrothermal mineral seal at which the ductile-brittle transition
1017 occurs (note the ductile brittle transition is here exemplified as a layer, but rather
1018 correspond to progressive, dynamic (in space and time) transitional environment
1019 from ductile rocks to brittle rocks and therefore a permeability transition).
1020 Seismicity (stars) and deformation (dashed line + arrows) patterns are also
1021 schematically illustrated. Time is in arbitrary units, and the chemical changes are
1022 purely hypothetical and for illustration purposes only. A recommended progression
1023 of geochemical monitoring actions is illustrated in the top panels. A continuous
1024 instrumental monitoring network is critically demanded to capture short-term
1025 changes prior to eruption, and to follow/monitor ongoing eruptions. This network
1026 should also ideally be in place at any SVGE (at both mafic open-vent volcanoes
1027 and more silicic dome-hosting volcanoes).

1028 Time (relative scale)